

# 1 Storylines of Summer Arctic climate change constrained by Barents-Kara Sea and 2 Arctic tropospheric warming for climate risks assessment

3 Xavier J. Levine<sup>1</sup>, Ryan S. Williams<sup>2</sup>, Gareth Marshall<sup>2</sup>, Andrew Orr<sup>2</sup>, Lise Seland Graff<sup>3</sup>, Dörthe  
4 Handorf<sup>4</sup>, Alexey Karpechko<sup>5</sup>, Raphael Köhler<sup>4</sup>, René Wijngaard<sup>6</sup>, Nadine Johnston<sup>2</sup>, Hanna Lee<sup>7,1</sup>, Lars  
5 Nieradzki<sup>8</sup>, Priscilla A. Mooney<sup>1</sup>

6 <sup>1</sup>Norwegian Research Centre, 5004 Bergen, Norway

7 <sup>2</sup>British Antarctic Survey, CB3 0ET Cambridge, United Kingdom

8 <sup>3</sup>Norwegian Meteorological Institute, 0371 Oslo, Norway

9 <sup>4</sup>Alfred Wegener Institute, 14473 Potsdam, Germany

10 <sup>5</sup>Finnish Meteorological Institute, FI-00560 Helsinki, Finland

11 <sup>6</sup>Utrecht University, 3584 CS Utrecht, The Netherlands

12 <sup>7</sup>Norwegian University of Science and Technology, 7491 Trondheim, Norway

13 <sup>8</sup>Lund University, 221 00 Lund, Sweden

14 *Correspondence to:* Xavier J. Levine ([xale@norceresearch.no](mailto:xale@norceresearch.no))

## 15 **Abstract**

16

17 While climate models broadly agree on the changes expected to occur over the Arctic with global warming on a pan-Arctic  
18 scale (i.e., polar amplification, sea-ice loss, increased precipitation), the magnitude and patterns of these changes at regional  
19 and local scales remain uncertain. This limits the usability of climate model projections for risk assessments and their impact  
20 on human activities or ecosystems (e.g., fires, permafrost thawing). Whereas any single or ensemble-mean projection may be  
21 of limited use to stakeholders, recent studies have shown the value of the storyline approach in providing a comprehensive and  
22 tractable set of climate projections that can be used to evaluate changes in environmental or societal risks associated with  
23 global warming.

24 Here, we apply the storyline approach to a large ensemble of CMIP6 models, with the aim of distilling the wide spread in  
25 model predictions into four physically plausible outcomes of Arctic summertime climate change. This is made possible by  
26 leveraging strong covariability in the climate system, associated with well-known but poorly constrained teleconnections and  
27 local processes: specifically, we find that differences in Barents-Kara Sea warming and lower tropospheric warming over polar  
28 regions among CMIP6 models explain most of the inter-model variability in pan-Arctic surface summer climate response to  
29 global warming. Based on this novel finding, we compare regional disparities in climate change across the four storylines. Our  
30 storyline analysis highlights the fact that, for a given amount of global warming, certain climate risks can be intensified while  
31 others may be lessened, relative to a “middle-of-the-road” ensemble mean projection. We find this to be particularly relevant  
32 when comparing climate change over terrestrial and marine areas of the Arctic, which can show substantial differences in their

33 sensitivity to global warming. We conclude by discussing potential implications of our findings for modelling climate change  
34 impacts on ecosystems and human activities.

## 35 **1 Introduction**

36 Since the late twentieth century, the surface of the Arctic has warmed 2 to 4 times greater than the global average, which is  
37 referred to as Arctic amplification (hereinafter AA, e.g., Jansen et al., 2020; England et al., 2021; Rantanen et al., 2022). This  
38 warming amplification of the near-surface and troposphere is caused by a number of feedbacks involving oceanic, cryospheric  
39 and atmospheric processes (Previdi et al., 2021). Sea-ice cover loss in the Arctic Ocean explains the bulk of the near-surface  
40 warming, especially over marine areas and coastal terrestrial regions due to its impact on surface energy fluxes and upper  
41 ocean warming (e.g., Screen and Simonds, 2010; Dai et al., 2019; Jenkins and Dai, 2021). Sea-ice loss and sea surface warming  
42 have been singularly strong in the Barents-Kara Sea, which has been identified as a warming hotspot (Lind et al. 2018) and a  
43 mediator of climate change between the North Atlantic and Central Arctic Oceans (Smedsrud et al., 2013). AA is also tied to  
44 tropospheric warming, which is influenced to a greater extent by atmospheric dynamical feedback, such as temperature  
45 feedbacks (Pithan and Mauritsen, 2014) and poleward atmospheric energy transport feedback (e.g., Merlis and Henry, 2018).  
46 Overall, the combined influence of oceanic, cryospheric and atmospheric processes render Arctic climate change and its  
47 surface warming amplification especially complex to predict.

48  
49 AA has resulted in extensive loss of land ice, snow cover, and thawing of the permafrost over the Arctic region (e.g., Callaghan  
50 et al., 2011; van den Broeke et al., 2016; Chadburn et al., 2017; Shepherd and IMBIE Team, 2020). These profound changes  
51 to the Arctic climate system have been linked to increases in a range of societal and ecological risks (Yumashev et al., 2019).  
52 For example, past decades have shown an increase in the frequency and intensity of wildfires in many Arctic regions, such as  
53 North America's boreal forests (Masrur et al., 2018; McCarty et al., 2021), which has been attributed to unusually warm and  
54 dry spring and summer weather conditions (Krikken et al., 2019) as well as increased lightning activity (Veraverbeke et al.,  
55 2017). Likewise, the accelerated thawing of permafrost over large swathes of the terrestrial Arctic poses significant challenges  
56 for the integrity of local infrastructure, such as roads and buildings (Hjort et al., 2022). Impacts of climate change in the Arctic  
57 also extend to marine areas. For example, while increased sunlight in the photic zone from sea-ice loss and warmer sea surface  
58 temperature may have boosted marine primary production in the Arctic oceans in past decades (Arrigo and Van Dijken, 2015),  
59 evidence suggests that this is primarily benefiting species typically found at lower latitudes at the expense of native Arctic  
60 species (Ingvaldsen et al., 2021). Changes to the Arctic climate system have also been suggested to have caused an increase in  
61 the frequency and intensity of certain extreme weather over the Northern Hemisphere mid-latitudes (Cohen et al., 2014),  
62 although the mechanisms of action and broader importance of such polar-to-midlatitude teleconnections remain controversial  
63 (Vavrus, 2018). The loss of glaciers / land ice from Greenland, through both increased surface meltwater runoff and increased

64 glacier flow / dynamic ice loss, has been a major contributor to increased global sea-level rise (e.g., Rignot et al., 2011; Shepard  
65 and IMBIE team, 2020).

66

67 Assessing the many impacts of climate change in the Arctic requires a strong understanding of the physical state of the  
68 atmosphere, ocean, and sea ice, and how it will respond to climate change. This, however, has been hampered by future climate  
69 projections from global coupled climate models showing a wide range of possible outcomes (Overland et al., 2019; Notz et  
70 al., 2020; McCrystall et al., 2021; IPCC, 2021), which stems from uncertainties in possible future greenhouse gas emission  
71 scenarios, an incomplete understanding of key climate processes and their imperfect representation in models (model  
72 uncertainty), and natural (internal) variability within the climate system (Hawkins and Sutton, 2009). This lack of certainty  
73 poses considerable challenges for the planning and implementation of effective mitigation strategies by stakeholders impacted  
74 locally or remotely by Arctic climate change. The issue is often poorly addressed through the use of either a single-model or  
75 multi-model mean climate projection (Shepherd et al., 2018).

76

77 The storyline approach overcomes the limitations of the above approaches by identifying and describing physically plausible  
78 and self-consistent pathways that are representative of future climate change, which may be more helpful to develop mitigation  
79 strategies (Shepherd et al., 2018). Storylines express the response of the Arctic climate to global warming conditional on a  
80 range of environmental conditions being realised. They are based on a methodology recently developed for studying the impact  
81 of climate change in other areas, primarily in the midlatitudes, e.g., western and central Europe (Zappa and Shepherd, 2017  
82 [ZS17]) or Southern Hemisphere midlatitude regions (Mindlin et al., 2020 [M20]). In this study, we posit that a substantial  
83 fraction of the variability of the surface climate response to global warming in the Arctic is associated with the warming of the  
84 Barents-Kara Sea and the warming of the Arctic lower troposphere. This is borne out of Barents-Kara Sea warming and the  
85 lower tropospheric warming being strongly influenced by climate variability at lower latitudes, but also being key players in  
86 driving surface warming in the Arctic. The Barents-Kara Sea, while being sensitive to changes in the Atlantic storm track  
87 (Jung et al., 2017) and the tropics (Warner et al., 2020), have long been recognised as a key modulators of climate variability  
88 in Earth's Northernmost regions (Li et al., 2020; Peings et al., 2023). Likewise, the warming of the Arctic lower troposphere,  
89 which is sensitive to changes in poleward atmospheric heat transport from lower latitudes (Russotto and Biasutti, 2020),  
90 strongly influences the near-surface climate through its impact on the boundary layer stability and surface radiative forcing  
91 (e.g., Previdi et al., 2020).

92

93 Using a range of possible scenarios for the Barents-Kara Sea and Arctic lower tropospheric warming that emerge from climate  
94 model simulations, we devise storylines of future climate change for Arctic regions. Specifically, we compare the climate of  
95 the last 30 years of the 21st century (2070–2099) projected in a high-end global warming scenario (corresponding with 8.5 W  
96 m<sup>-2</sup> additional increase in radiative forcing by 2100 relative to preindustrial, the Shared Socioeconomic Pathways 5-8.5, SSP5-  
97 8.5; see O'Neill et al. 2016 and Meinshausen et al., 2020), with the last 30 years of the historical experiment (1985–2014).

98 SSP5-8.5 represents the upper boundary of the range of scenarios described in ScenarioMIP and is useful to obtain the strongest  
99 possible response to climate change within the framework of the CMIP6; this ensures that the impact of internal climate  
100 variabilities is minimised in our study. We focus on the summer season, due to its relevance to societal and ecological impacts  
101 at high-latitude that peak in the warm part of the year, such as, among others, high-latitude fires, trans-Arctic shipping, and  
102 marine primary production. After describing the dataset and methodology used for our storyline analysis in section 2, we  
103 describe in section 3 how our Arctic storylines differ from the multi-model ensemble mean response, as established by four  
104 target variables we identified as being most relevant for studying climatic impacts in the region. We discuss the relevance of  
105 our findings for evaluating climate impacts in the Arctic region in section 4.

## 106 **2 Data and Methodology**

### 107 **2.1 Model data**

108 Our analysis uses a set of 43 climate models from CMIP6, which we downloaded from The Earth System Grid Federation  
109 (ESGF; Cinquini et al., 2014; models with members are listed on Table 1). The model and number of ensemble members  
110 (given in parentheses) include: TaiESM1 (1), BCC-CMS2-MR (1), CAMS-CSM1-0 (2), CAS-ESM2-0 (2), FGOALS-f3-L,  
111 FGOALS-g3 (4), (1), IITM-ESM (1), CanESM5 (15), CanESM5-CanOE (3), CMCC-CM2-SR5 (1), CMCC-ESM2 (1),  
112 CNRM-CM6-1 (6), CNRM-ESM2-1 (5), ACCESS-CM2 (5), E3SM-1-0 (5), E3SM-1-1 (1), E3SM-1-1-ECA (1), EC-Earth3  
113 (15), EC-Earth3-CC (1), FIO-ESM-2-0 (3), INM-CM4-8 (1), INM-CM5-0 (1), IPSL-CM6-LR (7), MIROC-ES2L (10),  
114 MIROC6 (15), HadGEM3-GC31-LL (4), HadGEM3-GC31-MM (4), UKESM1-0-LL (5), MPI-ESM1-2-LR (15), MRI-  
115 ESM2-0 (6), GISS-E2-1-G (14), GISS-E2-2-G (5), GISS-E2-1-H (10), CESM2 (3), CESM2-WACCM (3), NorESM2-LM (1),  
116 NorESM2-MM (1), KACE-1-0-G (3), GFDL-CM4 (1), GFDL-ESM4 (1), NESM3 (2), CIESM (1), MCM-UA-1-0 (1). For  
117 each model, all ensemble members of the historical experiment that were extended into the SSP5-8.5 scenario are used, capped  
118 to a maximum of 15 members per model to limit computational resources needed to produce ensemble means for the few  
119 models that have many members. As most models only have a few members, setting a maximum of 15 members seems a  
120 reasonable trade-off for reducing internal variability while including as many models as possible. We find little difference in  
121 using only a single member or an ensemble-mean of members, as the climate projections are dominated by the effect of the  
122 climate forcing with only a small contribution from natural variability (see Fig. 1b). For each model, we produce a mean  
123 climatology of the ensemble members for both the historical and SSP5-8.5 experiment, in their respective period of evaluation  
124 (i.e., 1985-2014 and 2070-2099), to reduce the weight of internal variability in the climate projections. Therefore, every model  
125 is represented by one climate projection regardless of their number of members, whether it is a single member or an ensemble-  
126 mean of members.

127 **2.2 Multivariate Linear Regression Analysis**

128 The climate storyline approach is based on a multivariate linear regression (MLR) analysis that expresses the response to  
 129 global warming of any variable,  $Z$  (“target variable”), as a linear superposition of its response to changes in  $N$  climate indices,  
 130  $P_i$ , (“predictor index”). Following the methodology outlined in Zappa and Shepherd (2017), this can be expressed as:

131  
 132 
$$\Delta Z(x, m) = \overline{\Delta Z}(x) + \sum_{i=1}^N \beta_i(x) \widehat{\Delta P}_i(m) \quad (1a)$$

133 where  $\widehat{\Delta P}_i(m) = \Delta P_i(m) - \overline{\Delta P}_i$  (1b)

134 Here,  $\Delta Z$  defines changes in target variable  $Z$ ,  $\Delta P_i$  changes in predictor index  $P_i$ , and  $\beta_i$  is the response of variable  $Z$  to changes  
 135 in  $P_i$ . Note that the target variable  $Z$  varies both in space  $[x]$  and across models  $[m]$ , but predictor indices  $P_i$  only vary across  
 136 models; predictor indices are typically regional averages of variables that are tied to well-known physical features of the  
 137 climate.  $\overline{(\cdot)}$  defines a multi-model ensemble mean (MMM) and  $\widehat{(\cdot)}$  a deviation from the MMM;  $\Delta$  defines the difference in  
 138 climatology between the 2070–2099 (SSP5-8.5 emission scenario) and 1985–2014 (historical experiment) period, normalised  
 139 by a global warming index,  $(T_{ssp585} - T_{hist})$ , i.e.,

140 
$$\Delta X = \frac{(X_{SSP585} - X_{hist})}{(T_{SSP585} - T_{hist})} \quad (2)$$

141 Here,  $T$  is the annual global-mean 2 m air temperature, and  $X$  defines any target variable or predictor index. Normalisation  
 142 ensures that changes in target variables and predictor indices are not directly associated with changes in the global warming  
 143 index ( $GWI$ , with  $GWI = T_{SSP585} - T_{hist}$ ). Instead, the normalised response describes the variability in target variables or  
 144 predictor indices linked to the underlying changes in the dynamics of the atmosphere/ocean/ice triggered by global warming,  
 145 rather than the variability directly affected by the model's climate sensitivity.

146  
 147 Storylines are constructed using the coefficients  $\beta_i$  emerging from the MLR analysis (Eq. 1), which are compounded with a  
 148 standardised climate response for each predictor. In a 2-predictors MLR analysis, this amounts to the creation of 4 storylines  
 149 that are representative of the diversity in the climate change response across CMIP6 models:

150  
 151 A.  $\widehat{\Delta Z}_{-,+}(x) = s (-\beta_1(x) + \beta_2(x)) \gamma$ , (3a)

152 B.  $\widehat{\Delta Z}_{+,+}(x) = s (+\beta_1(x) + \beta_2(x)) \Gamma$ , (3b)

153 C.  $\widehat{\Delta Z}_{-,-}(x) = s (-\beta_1(x) - \beta_2(x)) \Gamma$ , (3c)

154 D.  $\widehat{\Delta Z}_{+,-}(x) = s (+\beta_1(x) - \beta_2(x)) \gamma$ , (3d)

155 where  $\Gamma = \frac{1}{2} \frac{1-r^2}{1-r}$  and  $\gamma = \frac{1}{2} \frac{1-r^2}{1+r}$ . (3e)

156 Here,  $s$  defines the standardised climate response, whose value is set to 1.26. This value is derived from a Chi-square  
157 distribution for 2 degrees of freedom and evaluated on the edge of the 80% confidence boundary region; this distribution is  
158 applied to the standardised intermodel spread in our 2 predictors from the large ensemble of CMIP6 simulations described in  
159 section 2.1. In simpler terms,  $s$  defines a standardised deviation from the MMM of equal magnitude in our 2 predictor indices,  
160 which we deem plausible and yet not so extreme to be unlikely, based on the projection spread across CMIP6 simulations. To  
161 account for a weak positive correlation between both predictor indices, the storylines in Eq. (3) also contain factors  $\Gamma$  and  $\gamma$ ,  
162 which depends on the correlation coefficient  $r$  (see M20 for more details).

163  
164 The MLR framework of Eq. (1) and (3) seeks to predict the inter-model variability in the projections, and not the multi-model  
165 ensemble mean climate response; this is borne out of our storylines' aim, that is to explore a range of possible climate  
166 realisations representative of the diversity in model projections. While the MLR framework is compatible with using any  
167 number of predictor indices, the exponential increase in storylines with the number of predictors ( $2^N$  storylines can be produced  
168 for a set of  $N$  predictors) prompts us to use as few predictors as necessary, to keep the number of storylines tractable. We limit  
169 ourselves to two predictors and four storylines, as our analysis demonstrates that this configuration can explain a large fraction  
170 of the intermodel spread in the warming response of the Arctic (Table 1).

### 171 **2.3 Choice of target variables**

172 Due to their relevance to a broad array of climate risks, we select 2 m temperature, precipitation rate, 850 hPa zonal wind, and  
173 sea-ice fraction as target variables for understanding the impact of Arctic climate change (Lee et al., 2002). Note that the 850  
174 hPa zonal wind is considered to be a good proxy of the near-surface wind while being less sensitive to the physical  
175 parameterization of surface processes (e.g., ZS17). This choice of variables is highly relevant to many key climate-driven risks  
176 in the Arctic, including wildfires, permafrost thawing, sea-ice loss, and marine heatwaves (Anisimov and Nelson, 1997; Pabi  
177 et al., 2008; Arrigo and Van Dijken, 2015; Melia et al., 2016). For instance, Arctic wildfires are sensitive to warm, dry, and  
178 windy conditions, which implies a dependence on near-surface air temperature, near-surface wind, and precipitation accrued  
179 during the warm season (Dowdy et al., 2010). We define 2 m temperature as our reference target variable because of its  
180 preponderance in driving those climate risks. This means that our storylines are optimised to represent the variability in the 2  
181 m temperature.

### 182 **2.4 Choice of predictor indices**

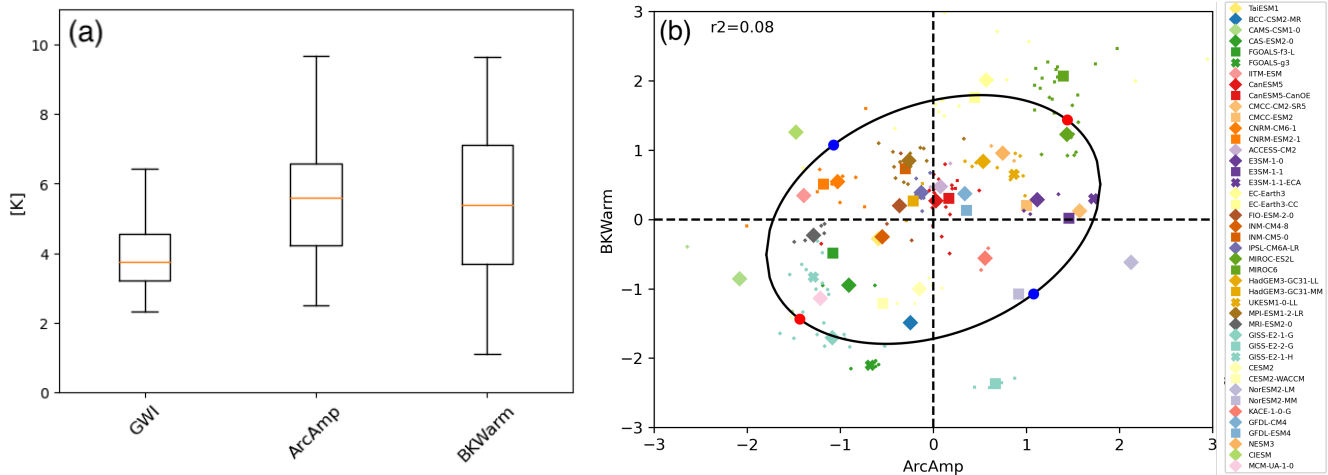
183 Using the MLR approach the target variables' response to global warming may be regressed upon the two climate indices that  
184 we consider optimal for explaining differences in climate change projections between the CMIP6 model simulations. In this  
185 study, we select Arctic atmospheric amplification and Barents-Kara Sea warming as our predictors, which we refer to  
186 respectively as 'ArcAmp' and 'BKWarm'. ArcAmp is defined as the 850 hPa temperature change averaged over all areas  
187 poleward of 55° N, and BKWarm as the sea-surface temperature change averaged over the Barents-Kara Sea (its outline is

188 shown on Fig. 2). Both ‘ArcAmp’ and ‘BKWarm’ are defined over the extended summer season (May to October). We choose  
189 these two predictors owing to their ability to explain a large fraction of the inter-model variability in climate change projections  
190 in the Arctic, specifically the warming of the boundary layer over marine and terrestrial regions. Indeed, comparing 850 hPa  
191 temperature against surface temperature in the Arctic regions shows a strong covariability over land but weak covariability  
192 over marine areas (see Fig. 2a,b), consistent with the thermal decoupling of the marine boundary layer from the free  
193 troposphere in summer (e.g., Tjernström and Graversen, 2009). Over ocean regions, the warming of the marine boundary layer  
194 is found to warm coherently across the Central Arctic, Barents-Kara, and North Atlantic regions (Fig. 2a), in agreement with  
195 a coherent increase in sea surface temperature across those regions. Due to its role as a climate gateway between the North  
196 Atlantic and the Arctic Ocean (e.g. Smedsrud et al., 2013), we select the Barents-Kara Sea as our reference region for defining  
197 our ocean warming predictor in the Arctic. Conversely, we select the 850 hPa Arctic mean temperature warming as our second  
198 predictor due to its high degree of covariability with the warming of the terrestrial boundary layer and low degree of  
199 covariability with the marine boundary layer warming (see Table B1). The processes tying temperature anomalies in the free  
200 troposphere to those of the surface over land likely involve multiple atmospheric feedback, such as radiative or boundary layer  
201 mixing changes, which is beyond the scope of this study. Likewise, while our study leverages the connections between the  
202 North Atlantic Ocean, Barents-Kara Sea and Central Arctic Ocean warming to produce a predictor for marine boundary layer  
203 warming (see Table B2), it does not seek to identify a mechanism connecting these three regions, as it would require an in-  
204 depth analysis of changes in ocean current, upper-ocean mixing, and surface fluxes.

### 205 **3 Results**

206 Figure (1a) shows the intermodel spread in ArcAmp, BKWarm and GWI, which is of comparable magnitude to their MMM  
207 value for all three indices; yet we note that the spread is larger for ArcAmp and BKWarm than GWI. This large spread reflects  
208 known uncertainties in the warming of the Barents-Kara Sea and the lower Arctic troposphere in climate models, which are  
209 associated with poorly constrained physical processes and teleconnections influencing the Arctic climate (e.g., Previdi et al.,  
210 2021). Figure (1b) shows ArcAmp and BKWarm for all CMIP6 models, which shows a weak correlation in their values ( $r^2 =$   
211 0.08); this is made evident by the elliptically shaped confidence boundary region on Fig. 1b, which accounts for the larger  
212 spread in variance along the direction of correlation (the ellipticity is determined by the  $\Gamma$  and  $\gamma$  factors in Eq. 3). This nearly  
213 satisfies an important condition of orthogonality necessary for the effective combined use of ArcAmp and BKWarm as  
214 predictors in the MLR framework (Eq. 1). The near independence in the changes of ArcAmp and BKWarm suggests that the  
215 sensitivity of the Barents-Kara Sea and that of the lower troposphere (850 hPa) to global warming are controlled by different  
216 physical processes--even if changes in both predictor indices are ultimately driven by global warming.

217



218  
 219 **Figure 1: (a) Boxplot showing the Global Warming Index (GWI), and the two predictor indices used for the storylines (ArcAmp and**  
 220 **BKWarm). GWI is defined as the global and annual-mean response of the 2 m temperature, ArcAmp the response of the 850 hPa**  
 221 **temperature averaged over all regions poleward of 55° N, and BKWarm the response of the sea surface temperature averaged over**  
 222 **the Barents-Kara Sea (units: K). Both ArcAmp and BKWarm are defined for the extended summer season (May to October).**  
 223 **Response is defined as the climatological-mean difference of the last 30 years of the current century (2070-2099) with that of the**  
 224 **historical period (1985-2014). The lowest and highest values are shown at the extremities of each box; box delimiters define the 25<sup>th</sup>**  
 225 **and 75<sup>th</sup> percentiles, while the median value (50<sup>th</sup> percentile) is shown by an orange line. (b) ArcAmp and BKWarm normalised by**  
 226 **the GWI and with the MMM value removed for each model. Note that each predictor index is rescaled by its standard deviation,**  
 227 **and thus non-dimensionalised (e.g., a value of 1 means a difference of one-standard deviation from the MMM value). The solid**  
 228 **ellipse delimits the 80% confidence region of the model response in ArcAmp and BKWarm (Eq. 3). Dots on the ellipse show the 4**  
 229 **storylines defined in Eq. (3a-d).**

230  
 231 Applying the 2-predictors MLR framework described in Eq. (1), we find that the inter-model variance in the 2 m temperature  
 232 explained by ArcAmp and BKWarm describes close to half of its overall inter-model variance over the Arctic (41%, see Table  
 233 1). This is about two-thirds of the theoretical maximum that can be explained using a 2-predictors MLR (64%), which we  
 234 evaluated as the variance explained by the first two components of a principal component analysis (PCA) applied on the  
 235 normalised change in 2 m temperature (Table 1; top row). Applying the same framework to explain changes in the 850 hPa  
 236 zonal wind, precipitation rate, and sea-ice fraction, we find that the amount of variance explained by our 2-predictors MLR is  
 237 substantially lower (~15%) for these variables, even if it is not insignificant. Nevertheless, evaluating the fraction of variance  
 238 explained by the MLR framework on regional-scale changes (either over the Arctic or broader Northern Hemisphere high  
 239 latitudes) generally indicates that our storylines have a larger explanatory power when applied to spatially coherent changes  
 240 in our target variables, strengthening the relevance of our Arctic storylines to variables other than 2-m temperature (Table 1;  
 241 bottom row). This highlights the fact that our storylines are tailored to quantitatively describe changes in the near-surface  
 242 warming and can only provide a qualitative picture of the changes in those three variables.



	<b>2 m temperature</b>	<b>850 hPa zonal wind</b>	<b>precipitation rate</b>	<b>sea-ice fraction</b>
<b>2-PCA variance [%]</b>	64	56	55	45
<b>MLR variance [%]</b>	41	14	18	12
<b>Arctic MLR variance [%]</b>	68	35	33	11

245 **Table 1: Explained variance for 2-m temperature, sea-ice fraction and precipitation rate over the Arctic (poleward of 55° N) and**  
 246 **850-hPa zonal wind over the Northern Hemisphere high latitude regions (poleward of 40° N) in the extended boreal summer (May**  
 247 **to October), expressed as a percentage of the total variance across model projections. Each column shows a target variable. The first**  
 248 **row is the amount of variance explained by the first 2 modes of a PCA on the respective target variable, which is the maximum**  
 249 **amount of variance that could be explained by a 2-predictors MLR. The second row is the amount of variance explained by our 2-**  
 250 **predictors MLR (Eq. 1), with ArcAmp and BKWarm as predictors. The third row is the amount of variance explained by our 2-**  
 251 **predictors MLR averaged over the Arctic (2-m temperature, precipitation rate, sea-ice fraction) and NH high latitude regions (850-**  
 252 **hPa zonal wind).**

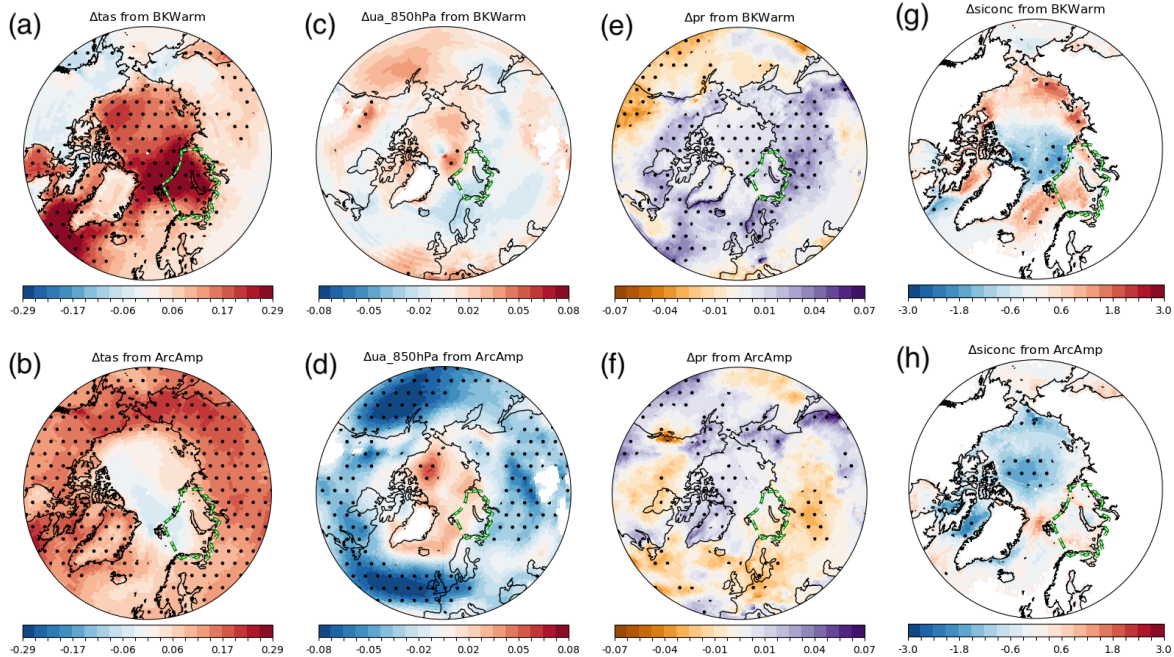
253

254 Figure 2 shows the normalised response of each target variable in the extended summer season to each predictor index, that is  
 255 the response per degree of global warming, for a one-standard deviation in the intermodel spread of the predictor index. A  
 256 warm anomaly in the Barents-Kara Sea (BKWarm) is associated with the following: a warm anomaly in the 2 m temperature  
 257 over the Central (marine) Arctic (Fig. 2a); a dipolar anomaly in the 850 hPa zonal wind changes, with weaker winds over the  
 258 Atlantic sector of the Arctic but stronger winds over the Pacific sector (Fig. 2c); positive anomalies in precipitation rates across  
 259 all Arctic regions, especially so over land areas (Fig. 2e); and accelerated rates of sea-ice loss in the Central Arctic, but reduced  
 260 rates of sea-ice loss the Pacific sector of the Arctic and Barents-Kara Sea (Fig. 2g). We note that sea-ice extent in the Barents  
 261 Sea region appears to be increasing in response to Barents-Kara Sea warming (Fig. 2g), a counter-intuitive finding that is likely  
 262 an artefact of the low number of models having sea-ice cover in summer in this region, as suggested by the lack of statistical  
 263 significance in the response.

264

265 These normalised response patterns strongly contrast with that associated with warm anomalies of the lower troposphere in  
 266 the Arctic (ArcAmp). For warm anomalies in ArcAmp, we find: 2 m temperature increases over most terrestrial areas (Fig.  
 267 2b); the 850 hPa zonal wind weakens over most areas around the Arctic but strengthens in the Central Arctic (Fig. 2d);  
 268 precipitation rates are reduced over most high-latitude land areas except over Greenland and the Bering Strait regions (Fig.  
 269 2f); and sea-ice loss is reduced in the Central Arctic and the Pacific sector of the Arctic basin (Fig. 2h). Both 2 m temperature  
 270 and precipitation rates response to ArcAmp are opposite to that associated with warm anomalies over the Barents-Kara Sea.

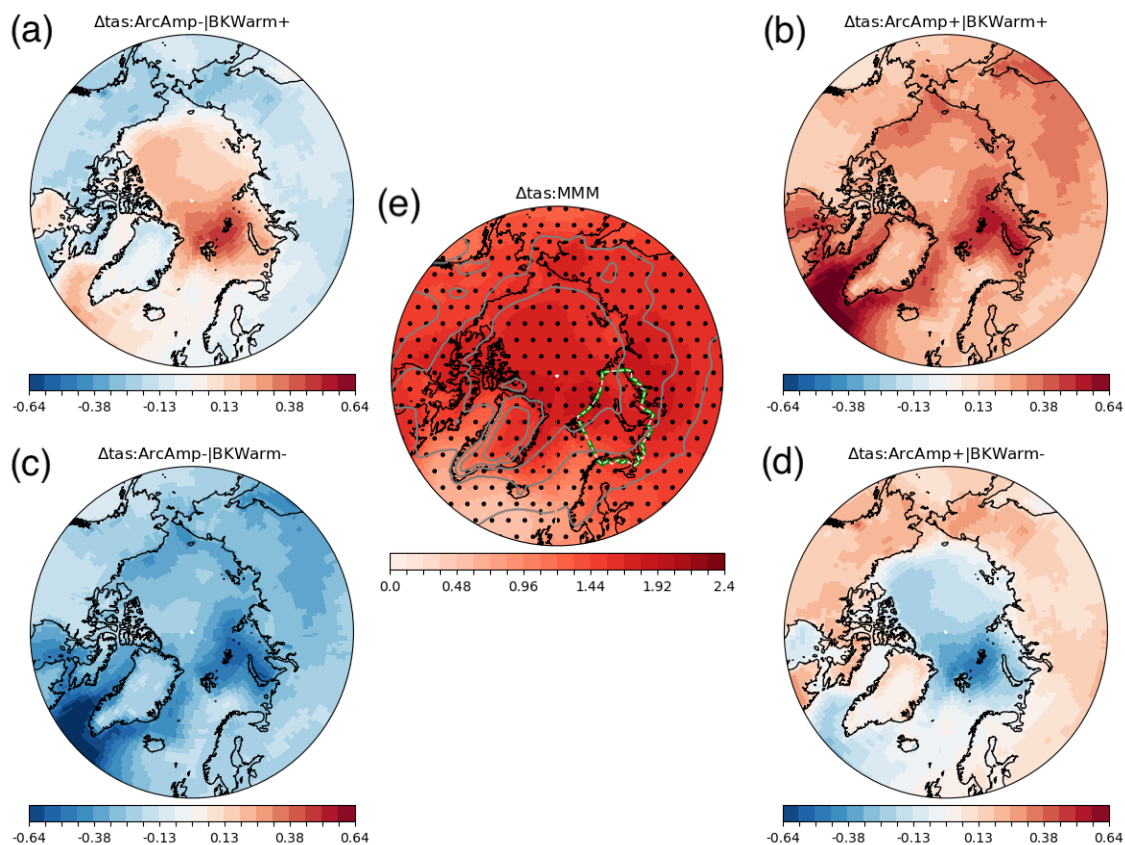
271 This difference in the normalised response to BKWarm and ArcAmp reflects important differences in how our two predictor  
 272 indices can modulate climate change and explain the diversity of model projections found under the SSP5-8.5 scenario  
 273 forcings.  
 274



275  
 276 **Figure 2: Normalised response of (from left to right) 2 m temperature [K K<sup>-1</sup>], 850 hPa zonal wind [m s<sup>-1</sup> K<sup>-1</sup>], precipitation rate [mm**  
 277 **day<sup>-1</sup> K<sup>-1</sup>], and sea-ice fraction [% K<sup>-1</sup>], to a one-standard deviation in each of the predictor index for BKWarm (top row) and**  
 278 **ArcAmp (bottom row). The normalised response is the product of the regression coefficient  $\beta_i$  in Eq. (1) with  $\sigma_{\Delta P_i}$ , a one-standard**  
 279 **deviation anomaly in the associated predictor index. Stippling indicates statistical significance at the 95% confidence level using**  
 280 **Student's t test (i.e., p-value less than 0.05). The green dashed line delineates the outline of the Barents-Kara Sea.**

281  
 282 Using these normalised responses to each predictor index, we produce four storylines for each of the four target variables  
 283 according to Eq. (3). Specifically, we describe the following four storylines, referenced from A to D and defined in Eq. (3): A:  
 284 ArcAmp- / BKWarm+, B: ArcAmp+ / BKWarm+, C: ArcAmp- / BKWarm-, D: ArcAmp+ / BKWarm-. Figure 3 shows  
 285 the storylines of 2 m temperature change. First, we note that the storylines' patterns are qualitatively similar to those obtained  
 286 from the two first modes of the PCA on 2 m temperature change (compare Fig. 3a-d with A1a-d); this confirms that our  
 287 ArcAmp and BKWarm predictors capture well the dominant modes of variability that drive the intermodel spread in surface  
 288 warming projections. Consistent with the normalised response patterns (Fig. 2a-b), the main difference in 2 m temperature  
 289 between the four storylines is the rate of warming between marine and terrestrial areas of the Arctic (Fig. 3). In the MMM, the  
 290 2 m temperature is found to increase by about 1.5 to 2 K K<sup>-1</sup> over most oceanic and terrestrial areas of the Arctic (Fig. 3e),

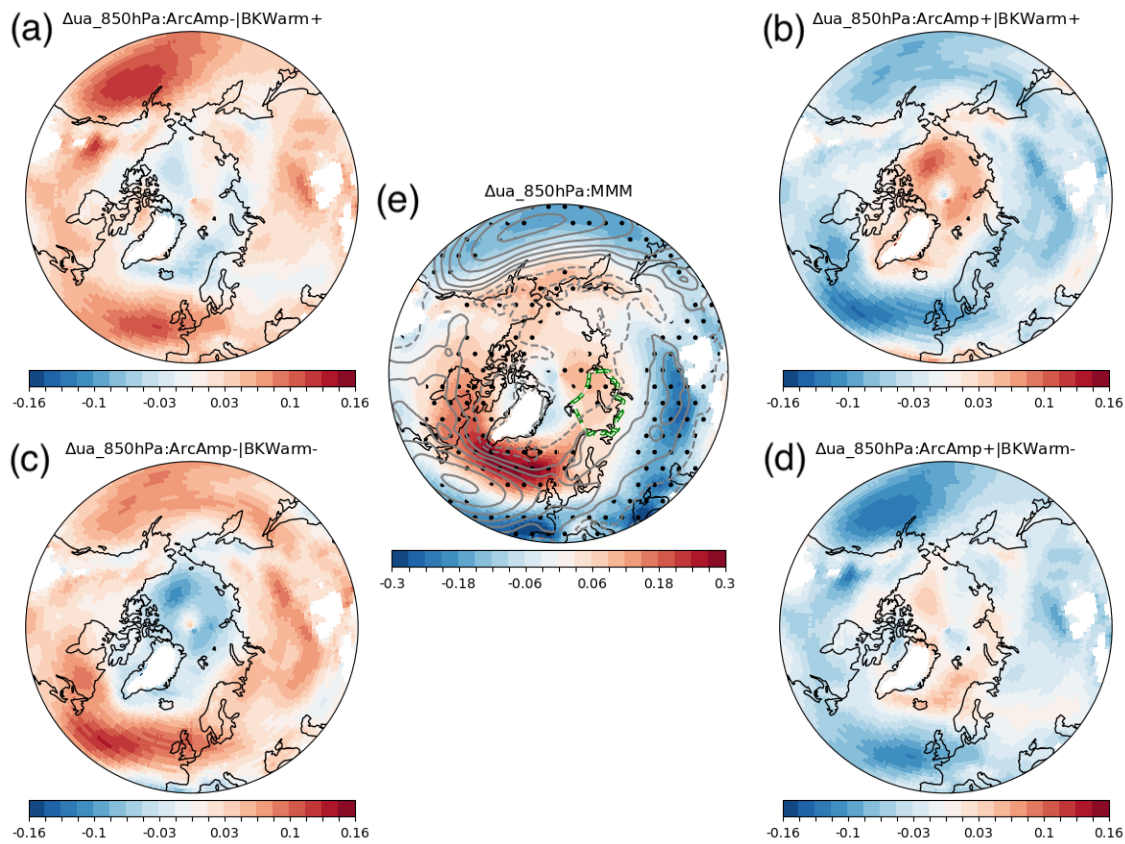
291 showing a relative uniformity in magnitude across the Arctic. For positive anomalies in both BKWarm and ArcAmp, i.e.,  
 292 storyline B, the rate of warming is increased over most Arctic areas (Fig. 3b); the opposite situation is found in storyline C,  
 293 i.e., negative BKWarm and ArcAmp anomalies, with a reduced rate of warming over most Arctic areas (Fig. 3c). For positive  
 294 (negative) anomalies in BKWarm but negative (positive) anomalies in ArcAmp, i.e., storyline A (D), the rate of warming is  
 295 increased (reduced) over marine areas but reduced (increased) over terrestrial areas when compared to the MMM (compare  
 296 Fig. 3a with 3d). Changes are stronger over marine areas, especially in the northern part of the Barents-Kara Sea and the  
 297 Western North Atlantic basin, where values can depart by up to 30% compared to the MMM. Out of all four storylines,  
 298 storylines A and D show the largest deviation in warming rates between terrestrial and marine areas (Fig. 3a,d). Beyond an  
 299 amplification or dampening of the MMM climate response, our analysis suggests a decoupling of the near-surface temperature  
 300 warming between terrestrial and marine areas, with the former being associated with the lower-tropospheric warming and the  
 301 latter connected to changes in the Barents-Kara and North Atlantic basin.  
 302



303  
 304 **Figure 3: (a)-(d) Storylines of climate change for 2 m temperature as defined in Eq. (3a-d) and (e) its MMM projection. Units: K K<sup>-1</sup>. Stippling on (e) indicates areas where at least 80% of the models agree on the sign of change, and grey solid contours indicate the**  
 305  
 306 **MMM present-day climatology. The green dashed line delineates the outline of the Barents-Kara Sea.**  
 307

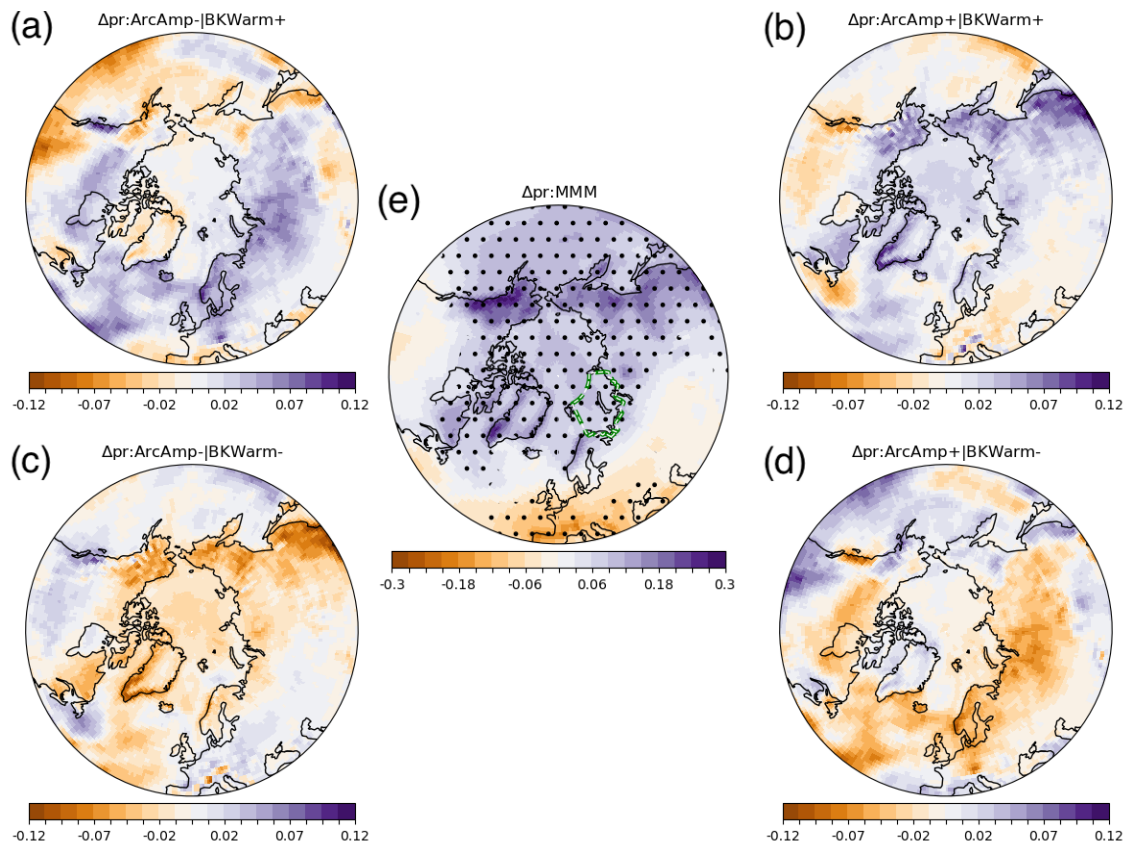
308 In comparison with the 2 m temperature, changes in the 850 hPa zonal wind show more complexity in the spatial pattern of  
309 changes between the four storylines. In the MMM, change in the 850 hPa zonal wind (U850) shows westerly tendencies across  
310 a wide area in the circumpolar regions, spanning eastward from the Bering Sea to the Barents-Kara Sea, with a maximum over  
311 the North Atlantic between Southern Greenland and Scandinavia. The westerly tendencies extend to the Pacific sector of the  
312 Arctic Ocean, forming an arch stretching from the Beaufort Sea to the Laptev Sea. On the other hand, easterly tendencies are  
313 found in the midlatitude regions of Central Siberia. Overall, those changes suggest that in the MMM, westerly winds shift  
314 poleward and strengthen around the subpolar front and in the Central Arctic, in qualitative agreement with previously noted  
315 changes in the Northern Hemisphere mid- and high-latitude regions (Harvey et al., 2020). Going beyond the multi-model mean  
316 changes, storylines indicate a strong modulation of those changes, with storyline changes being up to 50% of the MMM. As  
317 for the 2 m temperature, storylines of U850 show modulation of the MMM response departing from a simple amplification  
318 response. Storylines B and C show a bipolar pattern (Fig. 4b,c), with easterly (westerly) tendency in the circumpolar regions  
319 but westerly (easterly) tendencies over the Arctic ocean in B (C). Likewise, storylines A and D show an apparent bipolar  
320 pattern in climate response, with changes in the subpolar regions being of opposite signs of that found in the Norwegian and  
321 Barents Sea (Fig. 4a,d). Relative to the multi-model mean changes, the poleward shift in the North Atlantic storm tracks is  
322 influenced primarily by Arctic atmospheric warming, hence linking the large uncertainty in its prediction across climate models  
323 to the intermodel spread in ArcAmp. For instance, a strengthening of the 850 hPa zonal wind in the subpolar region occurs  
324 when ArcAmp weakens, consistent with polar atmospheric warming weakening the storm tracks (e.g. Smith et al., 2019). Even  
325 if our storylines account for only a fraction of the model spread in the 850 hPa zonal wind projections, the different outcomes  
326 outlined by our storylines suggest markedly different impacts of global warming on the low-level winds, with implications for  
327 changes in synoptic storms' tracks and intensity changes.

328



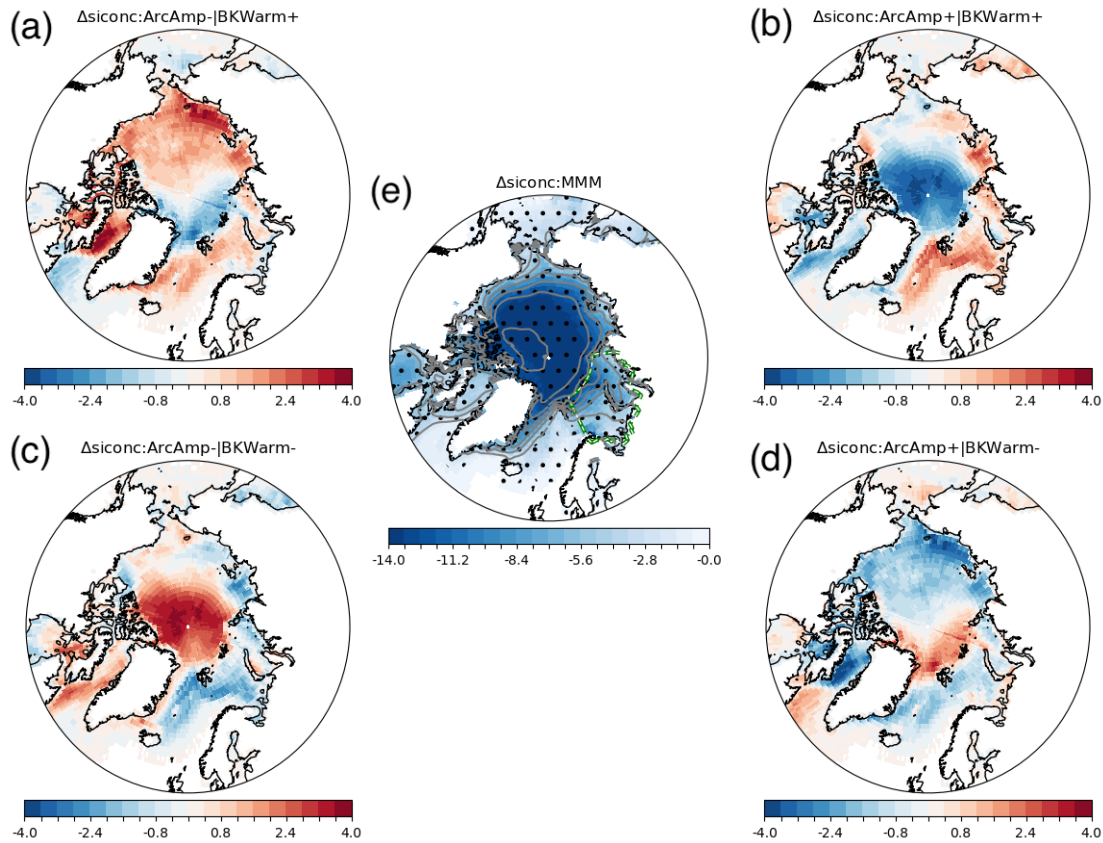
329  
 330 **Figure 4: Storylines of climate change for the 850 hPa zonal wind (a)-(d) and its MMM projection (e). Units: m s-1 K-1. Same**  
 331 **convention as Fig. 3 applies.**

332  
 333 Figure 5 confirms the expected increase in precipitation rate changes in the high-latitude regions, in the MMM. This increase  
 334 is most pronounced over mountain ranges found on the western sides of continents, which are on the paths of the Atlantic and  
 335 Pacific storm tracks, e.g., the North American coastal ranges, Western Greenland, Scandinavian coastal ranges (Fig. 5e). This  
 336 increase in precipitation rate contrasts with the drying tendency found over most of the midlatitude and subtropical regions of  
 337 Eurasia and North America. Storylines show that projections can differ substantially from this pattern, by up to 50% of the  
 338 MMM values. In particular, precipitation rate increases over most of the Arctic for positive anomalies in BKWarm (Fig. 5a,b),  
 339 but decreases for negative anomalies in BKWarm (Fig. 5c,d). Changes over terrestrial areas are generally of greater amplitude  
 340 than over marine areas across all storylines, and most particularly over regions of strong rainfall in the present-day climate.  
 341 Overall, storylines of precipitation rates are modulated primarily by change in BKWarm, with only specific regions--notably  
 342 Greenland and Siberia--showing a response to ArcAmp.



344 **Figure 5: Storylines of climate change for precipitation (a)-(d) and its MMM projection (e). Same convention as Fig. 3 applies.**  
 345  
 346

347 Figure 6 confirms the expected decline in sea-ice across the Arctic in the MMM, with sea-ice fraction displaying loss by at  
 348 least 15% (cf. Fig. 6e). However, our storylines reveal a more complex picture than suggested by the MMM. On one hand, a  
 349 Central Arctic amplification/dampening of these changes occur when BKWarm and ArcAmp changes are additive (Fig. 6b,c).  
 350 On the other hand, large regional contrasts can appear when BKWarm and ArcAmp changes are of opposite sign (Fig. 6a,d):  
 351 this is especially obvious when comparing the Atlantic and Pacific sector of the Arctic. Those changes appear to be associated  
 352 largely with the Arctic atmospheric warming, with the Barents-Kara Sea warming playing a more local role with its effect  
 353 being felt primarily in the Atlantic sector of the Arctic ocean.  
 354



355

356

**Figure 6: Storyline of climate change for sea-ice fraction (a)-(d) and its MMM projection (e).**

357

#### 4 Discussion and Conclusions

358

359

360

361

362

363

364

365

366

367

368

369

We produced four summertime climate change storylines for the Arctic region, for the four target variables that we consider to characterise seasonal change in the surface climate: 2 m temperature, precipitation rate, zonal wind at 850 hPa level, and sea-ice fraction over the Arctic region. We devised those storylines using an established methodology, previously applied to develop storylines across various midlatitude regions of both hemispheres (ZS17, ML20). We combined this framework with the realisation that Arctic climate change in summer is tightly associated with two climate indices, the Barents-Kara Sea warming (BKWarm) and Arctic atmospheric amplification (ArcAmp), which we used as predictors. Our choice of methodology and predictors was guided by two criteria: (i) our storylines should be representative of the diversity in model projections, and (ii) our predictors should be connected to physical processes. Criterion (i) ensures that the storylines capture a meaningful set of possible climate change realisations, while criterion (ii) allows for a scientific understanding of what drives this diversity in model projections. Criterion (i) is critical to the viewpoint of the end-users who need a plausible range of climate change scenarios, for instance to develop mitigation strategies, while criterion (ii) is of greater interest to scientists who desire insights regarding the drivers of climate change in the Arctic. When based on those two criteria, storylines can be

370 used to study possible impacts of climate changes, as well as categorise climate models by storylines; as such storylines are an  
371 efficient way of identifying a few climate models most representative of the diversity of CMIP6 projections.

372

373 Our storylines are particularly successful at capturing the spread in model projections for the 2 m temperature: our primary  
374 finding is the differential warming rates between terrestrial and marine areas, which we find to be a major source of divergence  
375 in model projections. We also applied our storyline analysis to other variables, to a varying degree of success: the relevance  
376 of storylines to each target variable must be assessed case-by-case, as different target variables may be controlled by distinct  
377 processes. Likewise, our predictors are less successful at capturing changes in seasons other than the extended boreal summer.  
378 The specificity of storylines to variables, seasons and regions is an important limitation of this methodology, as it relies on  
379 careful tuning to comprehensively represent changes.

380

381 Using this methodology, we produced the four Arctic climate change: ArcAmp- / BKWarm+ (A), ArcAmp+ / BKWarm+ (B),  
382 ArcAmp- / BKWarm- (C), ArcAmp+ / BKWarm- (D). Our storylines show noticeably different paths for Arctic climate  
383 change, which deviate substantially from the multi-model ensemble mean. Compared to the MMM, cooler surface temperature  
384 in storylines A and C suggests fewer fire risks and less extensive permafrost thawing, if undergoing the same amount of global  
385 warming. Storylines B and D present the opposite outcome, with more intense land warming that may lead to greater fire risks  
386 and more permafrost thawing. Concomitant changes in precipitation rates and surface wind are expected to modulate those  
387 trends: for instance, a wetter summer could imply a reduced fire risk in storyline B compared to D, even if both storylines  
388 show similar rates of warming over land. The combined impacts of physical changes at the surface on climate risks such as  
389 fires and permafrost thaw can only be evaluated with a quantitative analysis that is beyond the scope of our study. Furthermore,  
390 our analysis also shows that enhanced risks over land may or may not translate into enhanced impacts over marine areas. For  
391 instance, storyline A--which showed a lessening of climate risks over land---is tied to an enhanced warming of the Arctic  
392 Ocean and an amplified loss in sea-ice cover, suggesting a more navigable Arctic Ocean and greater disruptions in marine  
393 primary production compared to the MMM. Beyond changes that may be consistent across the entire Arctic, storylines also  
394 suggest futures in which regional contrasts are enhanced. For instance, storylines A and D show sea-ice cover shrinking may  
395 have pronounced differences between the Pacific and Atlantic sectors of the Arctic Ocean; such changes would likely entail  
396 regional differences in the volume of Arctic shipping or marine primary production. Overall, we demonstrate that storylines  
397 can be used to better understand the range of possible climate outcomes for the Arctic that emerge from coupled climate  
398 models, a critical step toward planning for climate adaptation strategies.



399 **Appendix A: Empirical storylines**

400 We also tested an empirical method for producing storylines, in which predictor indices emerge from a principal component  
 401 analysis (PCA). This is achieved by finding the first two components of a PCA applied to each target variable (von Storch and  
 402 Zwiers, 2002), and using those as predictors. Specifically, we can express changes in a target variable  $\Delta Z$  as:

403  
 404 
$$\Delta Z(x, m) = \overline{\Delta Z}(x) + \sum_{i=1}^N EOF_i(x) PC_i(m) \quad (A1)$$

405 Here,  $EOF_i$  is the eigenmode and  $PC_i$  the eigenvalues of the  $i$ -th mode, and the summation is done over  $N$  principal  
 406 components. As in the MLR storylines (Eq. 1), the PCA storylines describe the inter-model variability in model projections,  
 407 that is with respect to the MMM changes. Comparing the two frameworks, we find that eigenmode  $EOF_i(x)$  in Eq. (A1) is  
 408 analogue to coefficient  $\beta_i(x)$  in Eq. (1), and  $PC_i(m)$  in Eq. (A1) to climate predictor  $\Delta \hat{P}_i(m)$  in Eq. (1). Following the same  
 409 methodology to the physical storylines, we produce four “empirical” storylines:

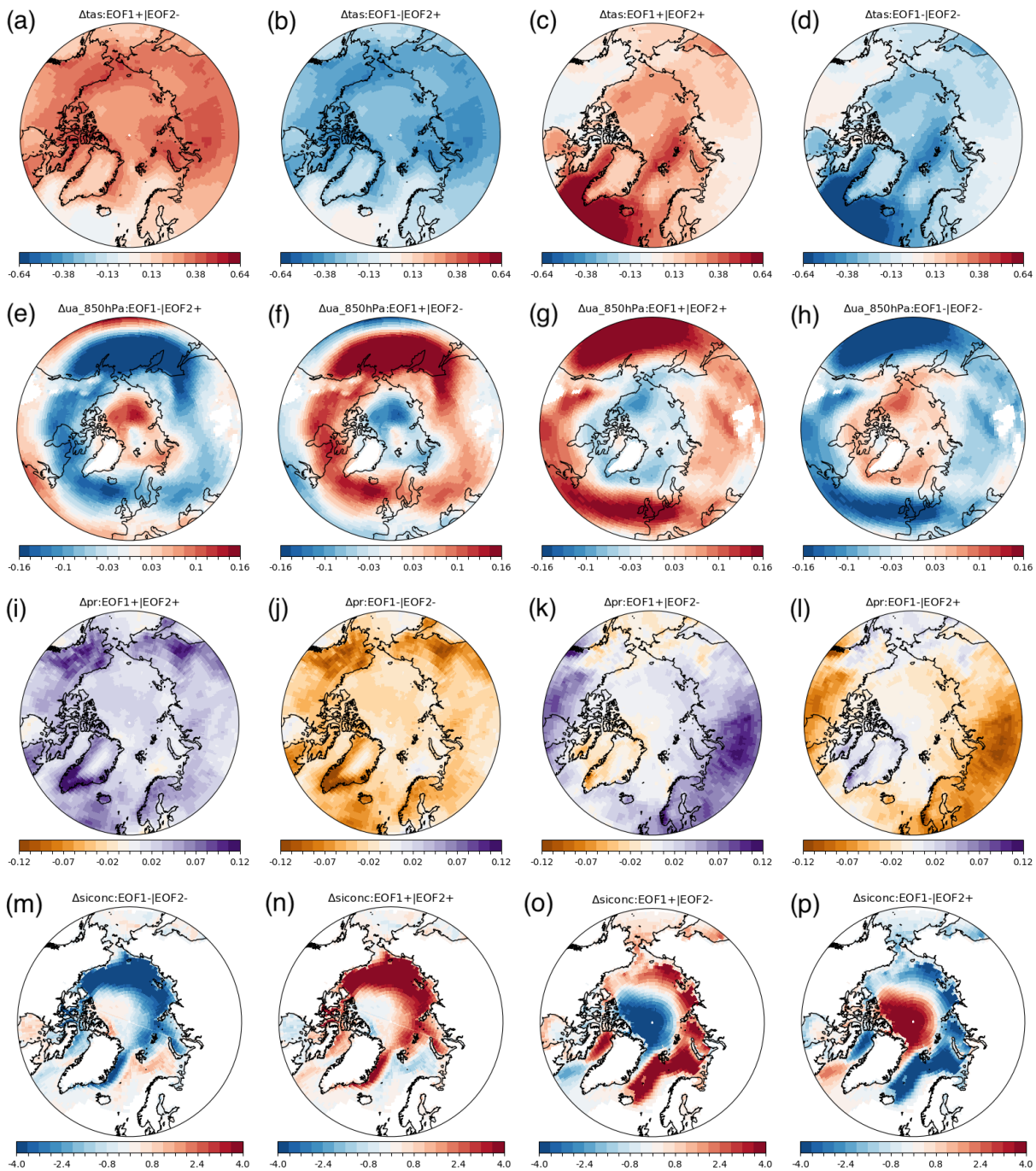
410  
 411 
$$\widehat{\Delta Z}_{+,+} = s(+EOF_1(x) + EOF_2(x)) \quad (A2a)$$

412 
$$\widehat{\Delta Z}_{+,-} = s(+EOF_1(x) - EOF_2(x)) \quad (A2b)$$

413 
$$\widehat{\Delta Z}_{-,+} = s(-EOF_1(x) + EOF_2(x)) \quad (A2c)$$

414 
$$\widehat{\Delta Z}_{-,-} = s(-EOF_1(x) - EOF_2(x)) \quad (A2d)$$

415 As in Eq. (3),  $s$  defines the standardised climate response in Eq. (A2), which is derived from a Chi-square distribution for 2  
 416 degrees of freedom and evaluated on the edge of the 80% confidence boundary region ( $s = 1.26$ ). Compared to the 2-predictors  
 417 MLR storylines (Eq. 3), the 2-components PCA storylines (Eq. A2) will better discriminate the spread in model projections,  
 418 since the variance explained by the first two components of a PCA maximises the variance that can be explained in the  
 419 intermodel spread from any two predictors. While PCA predictors present the advantage of being strictly orthogonal to each  
 420 other by construction, they are not directly relatable to specific climate indices or physical processes, which is a substantial  
 421 drawback for interpreting changes. For these reasons, empirical storylines may be useful for providing a representative range  
 422 of climate outcome to end-users (perhaps even more so than the MLR storylines, if judging solely from the amount variance  
 423 explained); however, they are likely to be less relevant for understanding the underlying processes driving the diversity in  
 424 climate outcomes.



425  
426 **Figure A1: EOF Storyline of climate change for: 2 m temperature, 850 hPa zonal wind, precipitation, and sea-ice fraction.**

427  
428 Empirical storylines show qualitative similarities with the storylines presented in our study (see Fig. A1) to those found in our  
429 physical storylines for most target variables (Fig. 3-6), even if physical storylines consistently underperform empirical ones

430 with regards to the amount of explained variance in model projections. This is particularly true for the 2 m temperature, which  
431 shows very similar patterns between empirical storylines and our storylines (compare Fig. A1 and 3).

## 432 **Appendix B: Optimizing Arctic storylines' predictors**

433 We selected the predictors for our Arctic storylines based on their ability to represent changes in key surface climate variables  
434 in a linear regression framework. This entails that our two predictors should maximize the variance explained by the MLR  
435 model while being as weakly correlated as possible (orthogonality of predictors is not strictly necessary but remains convenient  
436 for interpreting changes). We already motivated in Section 2.4 that lower tropospheric temperature change (represented by  
437 ArcAmp) and sea surface warming at high latitudes (represented by BKWarm) are the most relevant factors for defining our  
438 two predictors; however, we did not explain the specific choices of pressure level or area for evaluating ArcAmp or BKWarm.

439  
440 Table B1 shows the variance explained by the MLR model when using as predictors BKWarm (as defined in 2.4) and ArcAmp  
441 (as defined in 2.4 but using the pressure level value shown in top row); Table B1 also shows the correlation coefficient between  
442 BKWarm and ArcAmp at various levels.

443

	1000 hPa	925 hPa	850 hPa	700 hPa	600 hPa	500 hPa
Explained variance ( $R^2$ )	0.40	0.43	0.41	0.35	0.32	0.30
Predictors correlation ( $r^2$ )	0.38	0.14	0.08	0.05	0.06	0.09

444 **Table B1: (top row) Explained variance for the 2-m air temperature over the Arctic by the multivariate linear regression model,**  
445 **using BKWarm and ArcAmp as predictors, for various evaluation levels of ArcAmp. (bottom row) Correlation  $R^2$  of BKWarm with**  
446 **ArcAmp, for various levels of evaluation of ArcAmp (columns) ranging from the lowest model level (1000 hPa; leftmost column) to**  
447 **the mid-troposphere (500 hPa; rightmost column).**

448

449 Compared with other vertical levels, Table B1 shows that temperature at the 850 hPa level is only weakly correlated with the  
450 Barents-Kara sea warming (0.08, see bottom row in Table B1) and also nearly maximizes the MLR explained variance (0.41,  
451 see top row in Table B1). Specifically, MLR explained variance is found to decrease from a maximum value of 0.43 at 925  
452 hPa to lower values higher in the troposphere, while the predictor correlation decreases swiftly above the lowest tropospheric  
453 level (1000 hPa), which makes the 825 hPa level a reasonable choice for defining ArcAmp. We also note that the 825 hPa  
454 pressure level was selected to define Arctic Amplification in past studies (e.g., Manzini et al., 2014; ZS17).

455

456 Similarly to Table B1, we compare the variance explained by the MLR model and correlation coefficient when using as  
457 predictors ArcAmp (as defined in 2.4) and sea surface warming averaged over various areas of the Northern Hemisphere  
458 (including the Barents-Kara sea), as shown in Table B2. In addition to the Barents-Kara sea, we tested the Central Arctic and

459 North Atlantic ocean warming because of their covariability with Barents-Kara sea warming (Fig, 2a) and being areas where  
460 intermodel variability in sea surface warming is the strongest at high latitudes (Fig. A1, a-d).

461

	Barents-Kara Sea	Central Arctic Ocean	North Atlantic Ocean
Explained variance ( $R^2$ )	0.41	0.40	0.45
Predictor correlation ( $r^2$ )	0.08	0.09	0.13

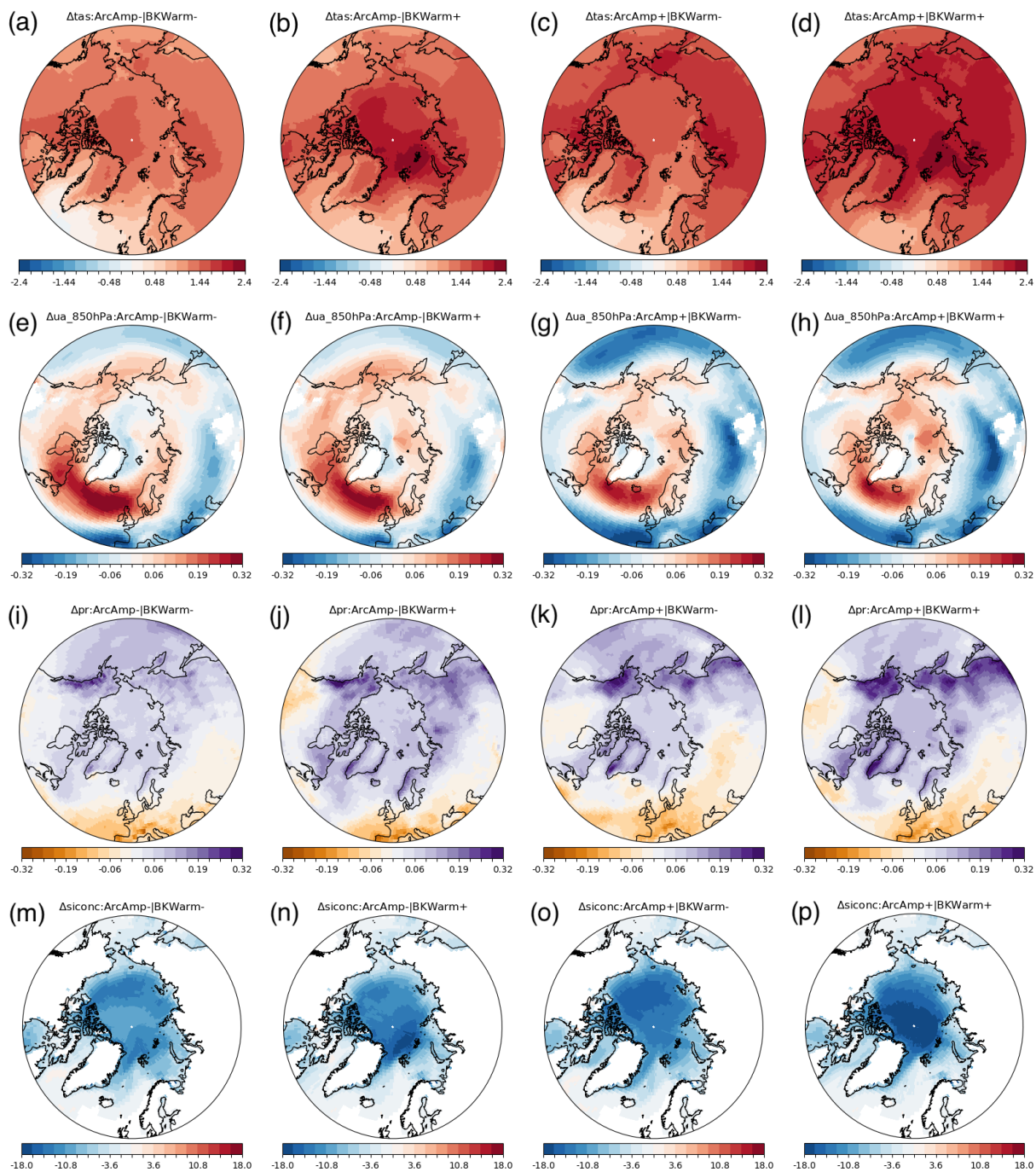
462 **Table B2: same as Table 1 but using various oceanic regions for our ‘BKWarm’ predictor: Barents-Kara sea (left column; [65°N,**  
463 **80°N, 26°E, 95°E]; ocean only), Central Arctic ocean (middle column; [70°N, 90°N, 180°W, 180°E]; ocean only), North Atlantic**  
464 **ocean (right column; [45°N, 60°N, 70°W, 0°]; ocean only).**

465

466 Table B2 shows similar values for the MLR explained variance and predictor correlation when selecting either Central Arctic,  
467 North Atlantic or Barents-Kara sea warming. Based on this criterion alone, any of those three region could have been chosen  
468 as predictors for our Arctic storylines. Ultimately, we selected the Barents-Kara Sea as the reference area for defining our  
469 predictor because of its mediating role between the North Atlantic and the Arctic Ocean warming (e.g. Smedsrud et al., 2013),  
470 as explained in Section 2.4.

### 471 **Appendix C: storyline patterns - including the multi-model mean change**

472 Nearly all studies using the storyline approach show the total storyline patterns (e.g. ZS17), which corresponds to the response  
473 of the target variables to each predictor added upon the multi-model mean (MMM) change. Showing the full response is most  
474 relevant to the end-users to study climate risks but can make it more challenging to distinguish what differentiate storylines,  
475 because storylines’ patterns are strongly influenced by the common MMM change. For convenience, we provide the total  
476 storyline patterns, defined by adding the MMM change (normalized by the global and annual-mean 2-m air temperature) to  
477 the storyline pattern defined in Eqns. 3a-d and shown in Figs. 3-6, for: 2-m air temperature (Fig. C1, a-d), 850 hPa zonal wind  
478 (Fig. C1, e-h), precipitation rate (Fig. C1, i-l), and sea-ice fraction (Fig. C1, m-p). We comment on what differs between  
479 storylines in Sections 3-4.



480

481

482

483

**Fig. C1:** “Overall storylines” of climate change for 2-m temperature, 850 hPa zonal wind, precipitation and sea-ice fraction. “Overall storylines” are defined by combining the multi-model ensemble mean change (Figs. 3-6, e) with our climate change storylines, as defined in Equation 3 and with patterns shown on panels a, b, c, d of Figures 3-6.

484 **Code availability**

485 The code to generate our Arctic storylines can be found on the first author's GitHub page  
486 ([https://github.com/xlevine/Storylines\\_Analysis\\_ESD](https://github.com/xlevine/Storylines_Analysis_ESD)).

487 **Data availability**

488 This study was based on World Climate Research Programme (WCRP)'s CMIP6 archived simulations, which can be found  
489 on The Earth System Grid Federation (ESGF). This data was stored locally on the National Infrastructure for Research Data  
490 (NIRD), a component of the Norwegian research infrastructure services (NRIS).

491 **Author contribution:**

492 XL performed the formal analysis and was responsible for the data presentation, supervised efforts leading to this work, and  
493 was responsible for the preparation of the manuscript. XL, RW, GM, AO, LG, DH were instrumental in setting the main goals  
494 and structure of this study and setting the storyline methodology. NJ, HL, LN provided important methodological inputs related  
495 to storylines' impact. RW, GM, AO, LG, DH, AK, RK, RW, NJ, HL, LN, PM helped with the preparation of this draft,  
496 providing critical comments. PM procured funding necessary to conduct this study and set the overarching goals of the  
497 PolarRES project that led to this study.

498 **Competing interests:**

499 The authors declare that they have no conflict of interest.

500 **Acknowledgements:**

501 We acknowledge the support of PolarRES (grant number 101003590), a project of the European Union's Horizon 2020  
502 research and innovation programme. Storage and computing resources necessary to conduct this analysis was provided by  
503 Sigma2 — the National Infrastructure for High Performance Computing and Data Storage in Norway (project NS8002K and  
504 NN8002K). The CMIP6 simulations used for this analysis were obtained from the Earth System Grid Federation (ESGF), an  
505 infrastructure supported by the World Climate Research Programme (WCRP).

506 **References**

507

508 Anisimov, O.A., and Nelson, F.E.: Permafrost zonation and climate change in the northern hemisphere: results from transient  
509 general circulation models, *Climatic Change*, 35, 241-258, 1997.

510 Arrigo, K.R., and van Dijken, G.L.: Continued increases in Arctic Ocean primary production, *Prog. Oceanogr.*, 136, 60-70,  
511 2015.

512 Callaghan, T.V., Johansson, M., Brown, R.D., Groisman, P.Y., Labba, N., Radionov, V., Barry, R.G., Bulygina, O.N., Essery,  
513 R.L., Frolov, D.M., and Golubev, V.N.: The changing face of Arctic snow cover: A synthesis of observed and projected  
514 changes, *Ambio*, 40, 17-31, 2011.

515

516 Chadburn, S.E., Burke, E.J., Cox, P.M., Friedlingstein, P., Hugelius, G., and Westermann, S.: An observation-based constraint  
517 on permafrost loss as a function of global warming, *Nature Clim. Change*, 7, 340–344, 2017.

518 Cinquini, L., Crichton, D., Mattmann, C., Harney, J., Shipman, G., Wang, F., Ananthakrishnan, R., Miller, N., Denvil, S.,  
519 Morgan, M., and Pobre, Z.: The Earth System Grid Federation: An open infrastructure for access to distributed geospatial data,  
520 *Future Gener. Comp. Sy.*, 36, 400-417, 2014.

521 Cohen, J., Screen, J.A., Furtado, J.C., Barlow, M., Whittleston, D., Coumou, D., Francis, J., Dethloff, K., Entekhabi, D.,  
522 Overland, J, and Jones, J.: Recent Arctic amplification and extreme mid-latitude weather, *Nature Geosci.*, 7, 627–637, 2014.

523

524 Dai A., Luo D., Song M., and Liu J.: Arctic amplification is caused by sea-ice loss under increasing CO<sub>2</sub>. *Nat Commun.*, 10,  
525 121, 2019.

526 Dowdy, A.J., Mills, G.A., Finkele, K., and de Groot, W.: Index sensitivity analysis applied to the Canadian forest fire weather  
527 index and the McArthur forest fire danger index, *Meteorol. Appl.*, 17, 298-312, 2010.

528 England, M.R., Eisenman, I., Lutsko, N.J., and Wagner, T.J.W.: The recent emergence of Arctic Amplification, *Geophys. Res.*  
529 *Lett.*, 48, e2021GL094086, 2021.

530 Eyring, V., Bony, S., Meehl, G.A., Senior, C.A., Stevens, B., Stouffer, R.J., and Taylor, K.E.: Overview of the Coupled Model  
531 Intercomparison Project Phase 6 (CMIP6) experimental design and organization, *Geosci. Model Dev.*, 9, 1937-1958, 2016.

532 Harvey, B.J., Cook, P., Shaffrey, L.C., and Schiemann, R.: The response of the northern hemisphere storm tracks and jet  
533 streams to climate change in the CMIP3, CMIP5, and CMIP6 climate models, *J. Geophys. Res.-Atmos.*, 125,  
534 p.e2020JD032701, 2020.

535

536 Hawkins, E., and Sutton, R.: The potential to narrow uncertainty in regional climate predictions, *B Am. Meteorol. Soc.*, 90,  
537 1095–1108, 2009.

538 Hjort, J., Streletskiy, D., Doré, G., Wu, Q., Bjella, K., and Luoto, M.: Impacts of permafrost degradation on infrastructure,  
539 *Nat. Rev. Earth Environ.*, 3, 24-38, 2022.

540 Ingvaldsen, R.B., Assmann, K.M., Primicerio, R., Fossheim, M., Polyakov, I.V. and Dolgov, A.V.: Physical manifestations  
541 and ecological implications of Arctic Atlantification, *Nat. Rev. Earth Environ.*, 2, 874-889, 2021.

542 Arias, P., Bellouin, N., Coppola, E., Jones, R., Krinner, G., Marotzke, J., Naik, V., Palmer, M., Plattner, G.K., Rogelj, J. and  
543 Rojas, M. (Eds): *Climate Change 2021: the physical science basis, Contribution of Working Group I to the Sixth Assessment*  
544 *Report of the Intergovernmental Panel on Climate Change, 2021.*

545

546 Jansen, E, Christensen, J.H., Dokken, T., Nisancioglu, K.H., Vinther, B.M., Capron, E., Guo, C., Jensen, M.F., Langen, P.L.,  
547 Pedersen, R.A., and Yang, S.: Past perspectives on the present era of abrupt Arctic climate change, *Nature Clim. Change.* 10,  
548 714–721, 2020.

549

550 Jenkins, M., and Dai, A.: The impact of sea-ice loss on Arctic climate feedbacks and their role for Arctic amplification,  
551 *Geophys. Res. Lett.*, 48, e2021GL094599, 2021.

552

553 Jung, O., Sung, M.K., Sato, K., Lim, Y.K., Kim, S.J., Baek, E.H., Jeong, J.H., and Kim, B.M.: How does the SST variability  
554 over the western North Atlantic Ocean control Arctic warming over the Barents–Kara Seas?, *Environ. Res. Lett.*, 12, 03402,  
555 2017.

556 Krikken, F., Lehner, F., Hausteiner, K., Drobyshev, I., and van Oldenborgh, G. J.: Attribution of the role of climate change in  
557 the forest fires in Sweden 2018, *Nat. Hazards Earth Syst. Sci.*, 21, 2169–2179, 2019.

558 Lee, H., Johnston, N., Nieradzki, L., Orr, A., Mottram, R.H., van de Berg, W.J., and Mooney, P.A.: Toward Effective  
559 Collaborations between Regional Climate Modeling and Impacts-Relevant Modeling Studies in Polar Regions, *B Am.*  
560 *Meteorol. Soc.*, 103, E1866-E1874, 2022.

561

562 Li, M., Luo, D., Simmonds, I., Dai, A., Zhong, L., and Yao, Y.: Anchoring of atmospheric teleconnection patterns by Arctic  
563 Sea ice loss and its link to winter cold anomalies in East Asia, *Int. J. Climatol.*, 41, 547-558, 2021.

564 Lind, S., Ingvaldsen, R.B., and Furevik, T.: Arctic warming hotspot in the northern Barents Sea linked to declining sea-ice  
565 import, *Nature Clim. Change*, 8, 634-639, 2018.

566

567 Manzini, E., Karpechko, A.Y., Anstey, J., Baldwin, M.P., Black, R.X., Cagnazzo, C., Calvo, N., Charlton-Perez, A.,  
568 Christiansen, B., Davini, P. and Gerber, E.: Northern winter climate change: Assessment of uncertainty in CMIP5 projections  
569 related to stratosphere-troposphere coupling. *J. Geophys. Res.-Atmos.*, 119, 7979-7998, 2014.

570



571 Masrur, A., Petrov, A.N., and DeGroot, J.: Circumpolar spatio-temporal patterns and contributing climatic factors of wildfire  
572 activity in the Arctic tundra from 2001–2015, *Environ. Res. Lett.*, 13, 014019, 2018.  
573

574 McCarty, J.L., Aalto, J., Paunu, V.-V., Arnold, S.R., Eckhardt, S., Klimont, Z., Fain, J.J., Evangelidou, N., Venäläinen, A.,  
575 Tchebakova, N.M., Parfenova, E.I., Kupiainen, K., Soja, A.J., Huang, L., and Wilson, S.: Reviews and syntheses: Arctic fire  
576 regimes and emissions in the 21st century, *Biogeosciences*, 18, 5053–5083, 2021.  
577

578 McCrystall, M.R., Stroeve, J., Serreze, M., Forbes, B.C., and Screen, J.A.: New climate models reveal faster and larger  
579 increases in Arctic precipitation than previously projected, *Nat Commun.*, 12, 6765, 2021.

580 Meinshausen, M., Nicholls, Z.R., Lewis, J., Gidden, M.J., Vogel, E., Freund, M., Beyerle, U., Gessner, C., Nauels, A., Bauer,  
581 N., and Canadell, J.G.: The shared socio-economic pathway (SSP) greenhouse gas concentrations and their extensions to 2500,  
582 *Geosci. Model Dev.*, 13, 3571-3605, 2020.

583 Melia, N., Haines, K., and Hawkins, E.: Sea ice decline and 21st century trans-Arctic shipping routes, *Geophys. Res. Lett.*, 43,  
584 9720-9728, 2016.

585 Merlis, T.M., and Henry, M., 2018. Simple estimates of polar amplification in moist diffusive energy balance models, *J.*  
586 *Climate*, 31, 5811-5824, 2018.

587 Mindlin, J., Shepherd, T.G., Vera, C.S., Osman, M., Zappa, G., Lee, R.W., and Hodges, K.I.: Storyline description of Southern  
588 Hemisphere midlatitude circulation and precipitation response to greenhouse gas forcing, *Clim. Dynam.*, 54, 4399-4421, 2020.

589 Notz, D., and Community S.I.M.I.P.: Arctic sea ice in CMIP6, *Geophys. Res. Lett.* 47, e2019GL086749, 2020.  
590

591 O'Neill, B.C., Tebaldi, C., Van Vuuren, D.P., Eyring, V., Friedlingstein, P., Hurtt, G., Knutti, R., Kriegler, E., Lamarque, J.F.,  
592 Lowe, J., and Meehl, G.A.: The scenario model intercomparison project (ScenarioMIP) for CMIP6, *Geosci. Model Dev.*, 9,  
593 3461-3482, 2016.  
594

595 Overland, J., Dunlea, E., Box, J.E., Corell, R., Forsius, M., Kattsov, V., Olsen, M.S., Pawlak, J., Reiersen, L.O., and Wang,  
596 M.: The urgency of Arctic change, *Polar Sci.*, 21, 6-13, 2019.

597 Pabi, S., van Dijken, G.L., and Arrigo, K.R.: Primary production in the Arctic Ocean, 1998–2006, *J. Geophys. Res.- Oceans*,  
598 113, 2008.

599 Peings, Y., Davini, P., and Magnusdottir, G.: Impact of Ural Blocking on Early Winter Climate Variability Under Different  
600 Barents-Kara Sea Ice Conditions, *J. Geophys. Res.-Atmos.*, 128, p.e2022JD036994, 2023.

601 Pithan, F., and Mauritsen, T.: Arctic amplification dominated by temperature feedbacks in contemporary climate models,  
602 *Nature Geosci.*, 7, 181-184, 2014.

603  
604 Previdi, M., Janoski, T.P., Chiodo, G., Smith, K.L., and Polvani, L.M.: Arctic amplification: A rapid response to radiative  
605 forcing, *Geophys. Res. Lett.* 47, p.e2020GL089933, 2020.  
606  
607 Previdi, M., Smith, K.L. and Polvani, L.M.: Arctic amplification of climate change: a review of underlying mechanisms,  
608 *Environ. Res. Lett.*, 16, 093003, 2021.  
609  
610 Rantanen, M., Karpechko, A.Y., Lipponen, A., Nordling, K., Hyvärinen, O., Ruosteenoja, K., Vihma, T., and Laaksonen, A.:  
611 The Arctic has warmed nearly four times faster than the globe since 1979, *Commun. Earth Environ.*, 3, 168, 2022.  
612  
613 Rignot, E., Velicogna, I., van den Broeke, M.R., Monaghan, A., and Lenaerts, J.T.M.: Acceleration of the contribution of the  
614 Greenland and Antarctic ice sheets to sea level rise, *Geophys. Res. Lett.*, 38, L05503, doi:10.1029/2011GL046583, 2011.  
615  
616 Russotto, R.D., and Biasutti, M.: Polar amplification as an inherent response of a circulating atmosphere: Results from the  
617 TRACMIP aquaplanets, *Geophys. Res. Lett.*, 47, p.e2019GL086771, 2020.  
618  
619 Screen, J., and Simmonds, I.: The central role of diminishing sea ice in recent Arctic temperature amplification, *Nature*, 464,  
620 1334–1337, 2010.  
621  
622 Shepherd, T.G., Boyd, E., Calel, R.A., Chapman, S.C., Dessai, S., Dima-West, I.M., Fowler, H.J., James, R., Maraun, D.,  
623 Martius, O., and Senior, C.A.: Storylines: an alternative approach to representing uncertainty in physical aspects of climate  
624 change, *Climatic Change*, 151, 555-571, 2018.  
625  
626 Smedsrud, L.H., Esau, I., Ingvaldsen, R.B., Eldevik, T., Haugan, P.M., Li, C., Lien, V.S., Olsen, A., Omar, A.M., Otterå, O.H.,  
627 and Risebrobakken, B.: The role of the Barents Sea in the Arctic climate system, *Rev. Geophys.*, 51, 415-449, 2013.  
628  
629 Smith, D.M., Screen, J.A., Deser, C., Cohen, J., Fyfe, J.C., García-Serrano, J., Jung, T., Kattsov, V., Matei, D., Msadek, R.  
630 and Peings, Y.: The Polar Amplification Model Intercomparison Project (PAMIP) contribution to CMIP6: investigating the  
631 causes and consequences of polar amplification. *Geosci. Model Dev.*, 12, 1139-1164, 2019.  
632  
633 The IMBIE Team: Mass balance of the Greenland Ice Sheet from 1992 to 2018, *Nature*, 579, 233–239, 2020.  
634  
635 Tjernström, M. and Gravensén, R.G.: The vertical structure of the lower Arctic troposphere analysed from observations and  
636 the ERA-40 reanalysis. *Q. J. R. Meteorol. Soc.*, 135, 431-443, 2009.

637 van den Broeke, M. R., Enderlin, E. M., Howat, I. M., Kuipers Munneke, P., Noël, B. P. Y., van de Berg, W. J., van Meijgaard,  
638 E., and Wouters, B.: On the recent contribution of the Greenland ice sheet to sea level change. *Cryosphere*, 10, 1933–1946  
639

640 Vavrus, S.J.: The influence of Arctic amplification on mid-latitude weather and climate. *Curr. Clim. Change Rep.*, 4, 238-249,  
641 2018.  
642

643 Von Storch, H. and Zwiers, F.W. (Eds): *Statistical analysis in climate research*. Cambridge University Press, Cambridge,  
644 United Kingdom, ISBN 0511010184, 484 pp., 2002.  
645

646 Veraverbeke, S., Rogers, B.M., Goulden, M.L., Jandt, R.R., Miller, C.E., Wiggins, E.B., and Randerson, J.T.: Lightning as a  
647 major driver of recent large fire years in North American boreal forests, *Nature Clim. Change*, 7, 529-534, 2017.  
648

649 Yumashev, D., Hope, C., Schaefer, K., Riemann-Campe, K., Iglesias-Suarez, F., Jafarov, E., Burke, E.J., Young, P.J.,  
650 Elshorbany, Y. and Whiteman, G.: Climate policy implications of nonlinear decline of Arctic land permafrost and other  
651 cryosphere elements, *Nat Commun.*, 10, 1900, 2019.

652 Warner, J.L., Screen, J.A., and Scaife, A.A.: Links between Barents-Kara sea ice and the extratropical atmospheric circulation  
653 explained by internal variability and tropical forcing, *Geophys. Res. Lett.*, 47, p.e2019GL085679, 2020.

654 Zappa, G., and Shepherd, T.G.: Storylines of atmospheric circulation change for European regional climate impact assessment,  
655 *J. Climate*, 30, 6561-6577, 2017.